

MICROSTRUCTURE AND *IN-SITU* SOLIDIFICATION ANALYSIS OF AL-CE-MG ALLOY

BY JOSHUA STROH AND DIMITRY SEDIAKO

The constant need to improve engine performance and fuel economy has led the automotive and aerospace industries to maximize the use of light-weight alloys. Aluminum (Al) alloys are becoming increasingly popular because of their high strength to density ratio and their great casting properties. Al alloys have become one of the most widely used alloys for the manufacturing of powertrain component such as engine heads, pistons and turbochargers [1-4].

Recently, the effects of rare earth (RE) additions, such as cerium (Ce), on Al alloys have been a focus because these additions tend to increase strength and produce higher temperature resistance, and these improvements have demonstrated in pistons and turbochargers, specifically.

Notably, a large increase in yield strength, up to 77%, and creep resistance at temperatures exceeding 300 °C was observed for an Al-Ce-Mg alloy in comparison to an Al-Cu based industrial alloy A206 [5-8].

Why Ce has such positive effects in Al-Ce-Mg is a subject of on-going research. One study indicates that part of the answer may be in the formation of secondary phases (e.g., $Al_{11}Ce_3$, or Al-Ce-Mg) [7], but much is still unknown about the microstructural characteristics (i.e., the effects of the phases present as well as the solidification kinetics) – knowledge needed for further developing high strength Al alloys.

Studying the microstructural characteristics of alloys is challenging because all methods have significant limitations, as many are only useful to study the surface. X-ray diffraction, for example, is limited to characterization of surface properties, which may be different from the bulk. Neutron beams, however, are highly penetrating in aluminum: 10% of the beam will penetrate as deeply as 30 cm. This penetrating power enables the design of

experiments to observe changes to microstructural properties *in situ*. Sediako *et al.* [9-13] have demonstrated *in situ* neutron diffraction (ND) can analyze the characteristics of Al alloy systems during solidification. These studies indicate that *in-situ* ND is precise and reproducible, and is advantageous over thermal analysis because it characterizes the solid growth of each phase in multiple crystallographic planes.

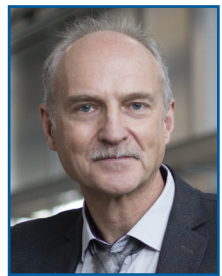
In this article, we illustrate the application of *in-situ* ND to Al alloys with current research to characterize the kinetics of solidification, phase evolution and fraction solid of several phases of Al-8%wt.%Ce-10wt.%Mg alloy. To obtain a fuller picture, ND is complemented with Optical Microscopy (OM), Scanning Electron Microscopy (SEM), and an equilibrium model FactSage™ simulation.

MICROSCOPY

To prepare for optical and electron microscopy, circular samples with an approximate diameter of 19 mm and a thickness of 12.5 mm were cut from a larger as-cast Al-Ce-Mg specimen, ground and polished and then submerged in Keller's etchant [14] for 30 seconds. Images were captured with the optical microscope at 100×, 200× and 500× magnification.

OM revealed six phases present in varying quantity throughout the continuous Al matrix, with approximate grains sizes from 50-200µm. SEM was then conducted to characterize the composition of each phase. Figure 1 illustrates several different phases that were further characterized with SEM techniques such as X-ray Energy Dispersive Spectroscopy (EDS) point analysis as well as secondary electron (SE) imaging. The SEM data obtained and the binary Al-Mg phase diagram suggest that the continuous matrix (location A in Fig. 1) is the α -aluminum containing dissolved magnesium, as well as Al-Mg phases (mostly Al_7Mg and $Al_{140}Mg_{89}$ [15-17]) phases with combined Mg concentration of approximately 13at.% (+/-2%).

Within the matrix was a “fish bone” secondary phase (location B) that ranged in size from 10-600 µm. This phase was determined to be composed of Al, Ce and Mg. The composition of a square or “X” (location C) shaped



Joshua Stroh
<josh_stroh@
alumni.ubc.ca>

and

Dimitry Sediako,
<dimitry.sediako@
ubc.ca>

School of
Engineering,
University of British
Columbia, 3333
University Way,
Kelowna, BC
V1V 1V7

SUMMARY

Higher performing or more efficient cars and planes challenge conventional approaches to understand and improve alloys. *In-situ* neutron diffraction reveals critical insights into alloys' microstructural evolution.

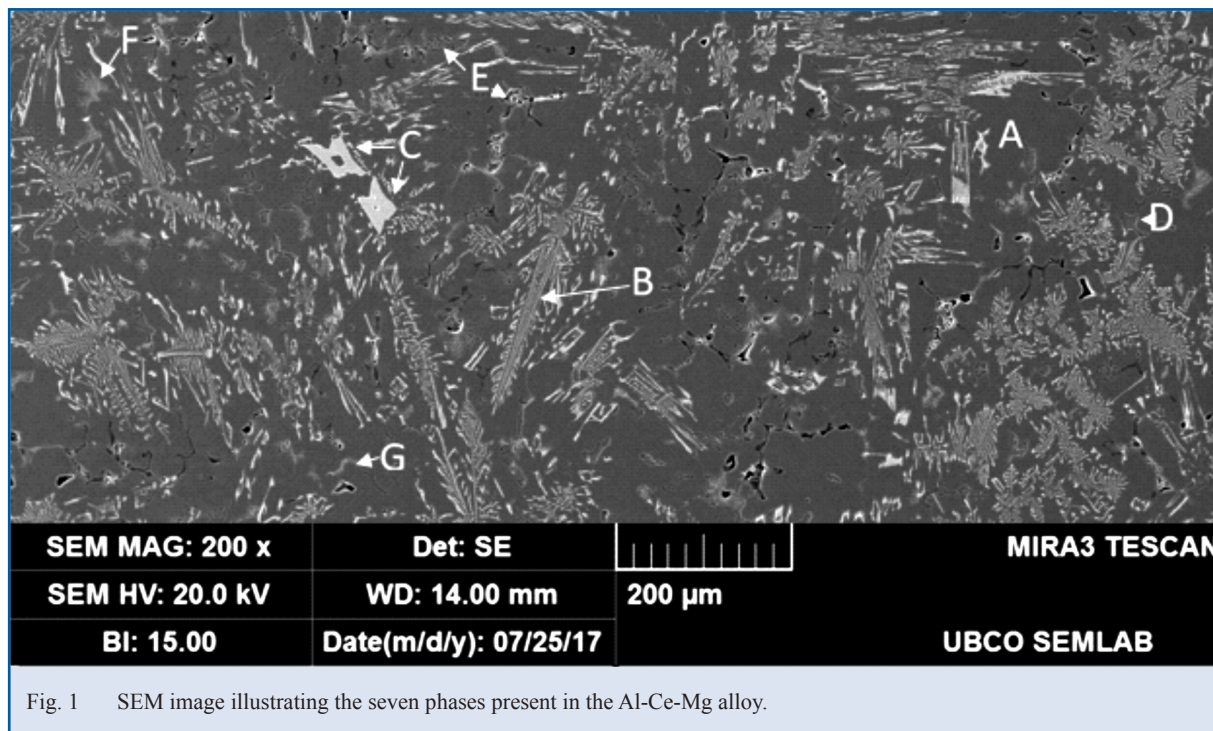


Fig. 1 SEM image illustrating the seven phases present in the Al-Ce-Mg alloy.

intermetallic was found to be similar to the $Al_{11}Ce_3$ phase of the Al-Ce-Mg alloy. A smaller, dark Chinese script phase (location E) as well as three different irregular shaped phases (locations D, F and G) were also present, but they appeared in lower quantity as compared to the fish bone phase.

NEUTRON DIFFRACTION

The *in-situ* ND experiments were performed at the C2 powder diffractometer at the Canadian Neutron Beam Centre (CNBC) in Chalk River, Ontario. To monitor temperature, a hole for a thermocouple was drilled in one end of a 10.5 mm diameter, 40 mm cylinder sample of the Al-Ce-Mg alloy. The sample was mounted into a graphite crucible and aligned within the furnace sample chamber to the neutron beam. Argon gas was used to minimise oxidation during the experiment. The methodology of the experiment is explained in more detail in [9-12].

To determine the range of temperature needed for the experiment, a FactSage™ simulation was used to predict the approximate liquidus, nucleation and solidification temperatures. The sample was elevated above the predicted liquidus temperature by ~25 °C to ensure the entire sample was completely molten. The temperature was then lowered stepwise and neutron diffraction data were collected for 1 hour at each step, using a monochromatic incident neutron beam with a wavelength of 2.37 Å, and a wide span detector collected neutron counts over a diffraction angle (2θ) range of 35° to 115°. The collection time represents a balance between the total beam time spent and the statistical quality of low intensity peaks for the

semi-solid metal at high temperatures. Applying Bragg's law for diffraction, as shown in Eq. (1), where n indicates the order of reflection, λ is the wavelength, and θ is the diffraction angle, the interplanar spacing d for various phases can be calculated [2,16],

$$n\lambda = 2d\sin\theta \quad (1)$$

Seven peaks were obtained from the ND data and analysed with application of the Inorganic Crystal Structures Database [18] based on the collected diffraction angles and corresponding d -values for the Al-Ce-Mg alloy. It was determined that three α -Al peaks ($\{111\}$, $\{200\}$ and $\{220\}$), three $Al_{11}Ce_3$ peaks ($\{103\}$, $\{112\}$, and $\{200\}$), and one Al-Ce-Mg peak were present.

As the metal is completely liquid at 610 °C, no noticeable peak is present at the first temperature step in Fig. 2. The next temperatures illustrate evolution of peak intensity. Figure 2 also illustrates a new phenomenon where the Bragg's peaks initially shift towards the left (i.e., smaller angles, larger d -spacing of the hkl -planes) until the temperature drops to ~530 °C, indicating an expansion in interplanar spacing, rather than a decrease as would be expected from thermal contraction and described by Lombardi *et al.* [4]. The reason for this unexpected shift has yet to be determined, but may be due to the secondary Al-Ce-Mg phase forming quite rapidly below approximately 570 °C (shown in Fig. 2), which takes place simultaneously with evolution of α -aluminum, and the atomic planes of the intermetallic phase may be affecting the hkl spacing of the aluminum matrix. Another possible reason for the angle shift is the rapid

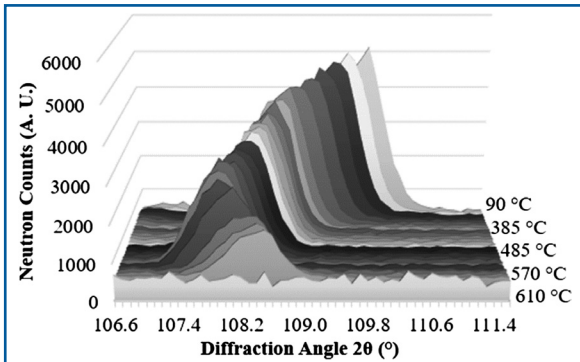


Fig. 2 Neutron diffraction peaks of the Al {220} plane in the Al-Ce-Mg alloy.

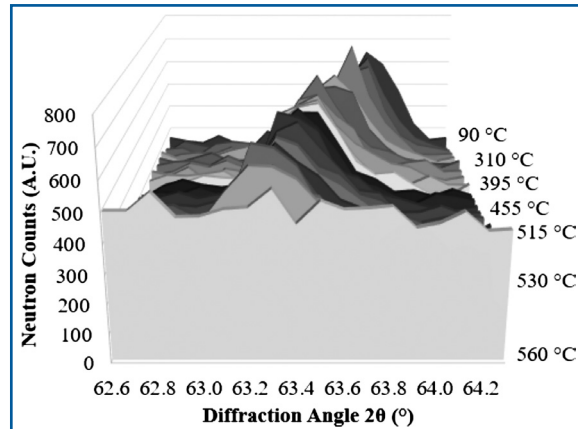


Fig. 3 Neutron diffraction peak of the "Fish bone" Al-Ce-Mg phase in the Al-Ce-Mg alloy.

increase in the amount of Mg dissolved in face centered cubic Al (FCC_Al) phase.

According to the FactSage™ simulation, the Mg begins precipitating out of FCC_Al at approximately 410 °C. This Mg precipitation contributes to the formation of the new Al-Ce-Mg phase, and further complicates the analysis. It especially complicates the Debye-Waller normalization, which is supposed to be temperature-dependant only [4]. Nonetheless, the simultaneous evolution of the Al-Ce-Mg, Al₁₁Ce₃, and the Al phases could increase the distance between adjacent lattice planes in the matrix and therefore cause the unexpected angular shift.

Figure 3 shows the peak corresponding to the low intensity Al-Ce-Mg secondary "fish bone" phase. The diffraction pattern for this phase is weak, with 13% of the intensity of the Al{220} plane, and no peak is clearly detectable until 530 °C, before which either the metal is fully liquid, which causes a relatively high background neutron count, or the phase has a very low volume fraction. In contrast, solid phases are visible in the data for Al₁₁Ce₃ at the highest temperature, 610 °C, even though the FactSage™ simulation predicted Al₁₁Ce₃ phase nucleation at ~560 °C. Thus, although FactSage™ properly predicted the primary the kinetics for α-Al phase, it misrepresented the evolution of Al₁₁Ce₃ phase.

While the location of the peaks corresponds to the interplanar spacing for a phase, the intensity of the peak is related to the fraction of the phase in the alloy, relative to the maximum amount of the phase (100%) at the completion of phase evolution. Integrating the peak intensities over the angular interval at the specific temperatures allows one to calculate the solidification kinetics for each of these phases. This calculation requires removing the background neutron scattering due to the graphite crucible or thermocouple materials, followed by normalizing against the peak intensity from liquidus to solidus.

Solidification curves similar to the representative trends shown in Fig. 4 were produced for each peak. The point at which a fraction solid of 1.0 is first reached was determined to be the end of

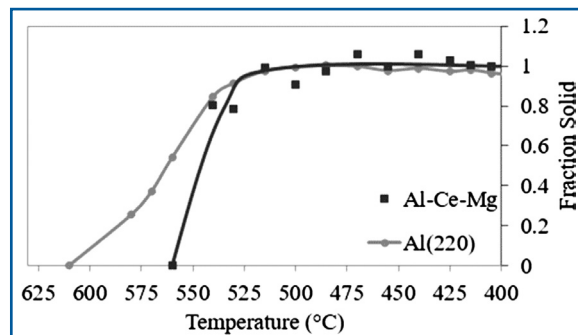


Fig. 4 Solidification curve of the Al (220) plane and the Al-Ce-Mg fish bone phase in the Al-Ce-Mg alloy (undetermined crystallographic plane).

evolution for that phase. For the Al-Ce-Mg alloy, the nucleation of the primary α-Al phase begins at temperatures above 580 °C and the phase continues to solidify until approximately 515 °C. Although the ND data indicated that the Al₁₁Ce₃ phase was still partially solid at the highest recorded temperature and therefore the exact nucleation temperature could not be determined, the end of solidification of this phase was found to be ~515 °C. The fraction solid curve of the new Al-Ce-Mg phase in Fig. 4 suggests that this phase begins nucleation at 560 °C and completes its solidification at 515 °C.

CONCLUSIONS

In-situ ND during the solidification of an Al-Ce-Mg alloy, complemented by microscopy analysis, provided a more comprehensive understanding of phase nucleation and evolution on multiple crystallographic planes. Though FactSage™ has been a reliable tool to get an understanding of the solidification path and primary and secondary phase evolution for systems, such as Mg-Al, Mg-Zn, Al-Cu, and Al-Si [2-4,11], it did not properly

predict the kinetics of phase evolution or the composition of the secondary phases in our Al-Ce-Mg alloy. This experiment provided data on evolution kinetics of Al-Ce and Al-Ce-Mg intermetallic phases that contribute to high yield strength at elevated temperatures, information that could lead to optimizing the composition and casting process for maximum strength. *In-situ* ND is therefore a powerful tool for the development of advanced alloys of interest to automotive and aerospace applications.

ACKNOWLEDGEMENTS

The authors gratefully acknowledge contribution of the sample material and expert support received from Dr. David Weiss of Eck Industries, Manitowoc, WI. We are also grateful to Canadian Nuclear Laboratories for neutron beam time. We acknowledge Dr. Daniel Banks of the Canadian Neutron Beam Centre for editing of the manuscript.

REFERENCES

1. N. Haghdadi, A.B. Phillion, and D.M. Maijer, "Microstructure Characterization and Thermal Analysis of Aluminum Alloy B206 During Solidification", *Metallurgical and Materials Transactions A*, **46A**, 2073-2081 (2015).
2. A. Elsayed, D. Sediako, and C. Ravindran, "Investigation of solidification behaviour of Mg-6Al and Mg-9Al alloys using *in-situ* neutron diffraction", *Can. Metall. Quart.* **54**, 17-25 (2015).
3. F. D'Elia, C. Ravindran, D. Sediako, and R. Donaberger, "Solidification analysis of Al5wt-%Cu alloy using *in-situ* neutron diffraction", *Can. Metall. Quart.* **54**, 9-16 (2015).
4. A. Lombardi, A. Elsayed, D. Sediako, and C. Ravindran, "Analysis of the solidification characteristics of a 319 type Al alloy using *in-situ* neutron diffraction", *Journal of Alloys and Compounds*, **695**, 2628-2636 (2017).
5. Y. Li, Z. Shi, Y.-L. Yang, B.-M. Huang, T.-F. Chung, and J.-R. Yang, "Experimental Investigation of tension and compression creep-aging behaviour of AA2015 with different initial tempers", *Material Science and Engineering A*, **657**, 299-308 (2016).
6. W.H. Li, X.F. Bian, H.Y. Li, and Y.F. Duan, "Interaction Between Rare Earth Ce and Hydrogen in Al-Cu Eutectic Alloy Melt", *Acta Metall. Sin.* **37**(8), 825-828 (2001).
7. D. Weiss, O. Rios, Z. Sims, S. McCall, and R. Ott, "Casting Characteristics of High Cerium Content Aluminum Alloys". Paper presented at the 146th TMS Annual Meeting, San Diego, California, 26 February – 2 March 2017.
8. B. Chevalier, and J.-L. Bobet, "On the Synthesis and Physical Properties of the IntermetallicsCeCuAl", *Intermetallics*, **9**(9), 835-838 (2001).
9. W. Kasprzak, D. Sediako, M. Sahoo, M. Walker, and I. Swainson, "Characterization of Hypereutectic Al-19%Si Alloy Solidification Process using *In-situ* Neutron Diffraction and Thermal Analysis Techniques", Proceedings of TMS, Supplemental Proceedings: *Materials Processing and Properties*, **1**, 93-104 (2010).
10. W. Kasprzak, D. Sediako, M. Walker, M. Sahoo, and I. Swainson, "Solidification Analysis of an Al-19 Pct Si Alloy Using *In-situ* Neutron Diffraction", *Metallurgical and Materials Transactions A*, **42A**, 1854-1862 (2011).
11. D. Sediako, and W. Kasprzak, "In-situ Study of Microstructure Evolution in Solidification of Hypereutectic Al-Si Alloys with Application of Thermal Analysis and Neutron Diffraction", *Metallurgical and Materials Transactions A*, **46A**, 4160-4173 (2015).
12. D. Sediako, W. Kasprzak, I. Swainson, and O. Garlea, "Solidification Analysis of Al- Si Alloys Modified with Addition of Cu Using *In-situ* Neutron Diffraction", Proceedings of the 146th TMS Annual Meeting, San Diego, California, 26 February – 2 March 2017, Supplemental Proceedings: *Materials Fabrication Properties, Characterization and Modeling*, **971**, 279-289 (2011).
13. F. D'Elia, C. Ravindran, D. Sediako, K.U. Kainer, and N. Hort, "Hot Tearing Mechanisms of B206 Aluminum-Copper Alloy", *Mater. Des.* **64**, 44-55 (2014).
14. J.R. Davis & Associates and ASM International Handbook Committee, Aluminum and aluminum alloys, ASM International, 1993.
15. T.B. Massalski, *Binary Alloy Phase Diagram*, 2 ed., vol.1, ASM Materials InformationSystem, 1992 (accessed 2017).
16. M. Mezbahul-Islam, A. Omar Mostafa and M. Medraj, "Essential Magnesium Alloys Binary Phase Diagrams and Their Thermochemical Data", *Journal of Materials*, **2014**, 33 (2014).
17. K. Fiz. In *Inorganic Crystal Structure Database*. <https://icsd.fiz-karlsruhe.de/>, 2017 (accessed 20 June 2017).